

Symmetry breaking and strong coupling in planar optical metamaterials

Koray Aydin^{1*}, Imogen M. Pryce¹, and Harry A. Atwater^{1,2}

¹Thomas J. Watson Laboratories of Applied Physics California Institute of Technology, Pasadena, California, USA

²Kavli Nanoscience Institute, California Institute of Technology, Pasadena, California, USA

*koray@caltech.edu

Abstract: We demonstrate narrow transmission resonances at near-infrared wavelengths utilizing coupled asymmetric split-ring resonators (SRRs). By breaking the symmetry of the coupled SRR system, one can excite dark (subradiant) resonant modes that are not readily accessible to symmetric SRR structures. We also show that the quality factor of metamaterial resonant elements can be controlled by tailoring the degree of asymmetry. Changing the distance between asymmetric resonators changes the coupling strength and results in resonant frequency tuning due to resonance hybridization.

© 2010 Optical Society of America

OCIS codes: (160.3918) Metamaterials; (220.4241) Nanostructure fabrication

References and links

1. E. Prodan, C. Radloff, N. J. Halas, and P. Nordlander, "A hybridization model for the plasmon response of complex nanostructures," *Science* **302**(5644), 419–422 (2003).
2. H. Wang, Y. P. Wu, B. Lassiter, C. L. Nehl, J. H. Hafner, P. Nordlander, and N. J. Halas, "Symmetry breaking in individual plasmonic nanoparticles," *Proc. Natl. Acad. Sci. U.S.A.* **103**(29), 10856–10860 (2006).
3. A. Christ, O. J. F. Martin, Y. Ekinci, N. A. Gippius, and S. G. Tikhodeev, "Symmetry breaking in a plasmonic metamaterial at optical wavelength," *Nano Lett.* **8**(8), 2171–2175 (2008).
4. N. Liu, H. C. Guo, L. W. Fu, S. Kaiser, H. Schweizer, and H. Giessen, "Plasmon hybridization in stacked cut-wire metamaterials," *Adv. Mater.* **19**(21), 3628–3632 (2007).
5. H. C. Guo, N. Liu, L. W. Fu, T. P. Meyrath, T. Zentgraf, H. Schweizer, and H. Giessen, "Resonance hybridization in double split-ring resonator metamaterials," *Opt. Express* **15**(19), 12095–12101 (2007).
6. F. Hao, Y. Sonnefraud, P. Van Dorpe, S. A. Maier, N. J. Halas, and P. Nordlander, "Symmetry breaking in plasmonic nanocavities: subradiant LSPR sensing and a tunable Fano resonance," *Nano Lett.* **8**(11), 3983–3988 (2008).
7. N. Verellen, Y. Sonnefraud, H. Sobhani, F. Hao, V. V. Moshchalkov, P. Van Dorpe, P. Nordlander, and S. A. Maier, "Fano resonances in individual coherent plasmonic nanocavities," *Nano Lett.* **9**(4), 1663–1667 (2009).
8. S. Zhang, D. A. Genov, Y. Wang, M. Liu, and X. Zhang, "Plasmon-induced transparency in metamaterials," *Phys. Rev. Lett.* **101**(4), 047401 (2008).
9. P. Tassin, L. Zhang, T. Koschny, E. N. Economou, and C. M. Soukoulis, "Low-loss metamaterials based on classical electromagnetically induced transparency," *Phys. Rev. Lett.* **102**(5), 053901 (2009).
10. N. Papasimakis, V. A. Fedotov, N. I. Zheludev, and S. L. Prosvirnin, "Metamaterial analog of electromagnetically induced transparency," *Phys. Rev. Lett.* **101**(25), 253903 (2008).
11. N. Liu, L. Langguth, T. Weiss, J. Kästel, M. Fleischhauer, T. Pfau, and H. Giessen, "Plasmonic analogue of electromagnetically induced transparency at the Drude damping limit," *Nat. Mater.* **8**(9), 758–762 (2009).
12. C. Enkrich, M. Wegener, S. Linden, S. Burger, L. Zschiedrich, F. Schmidt, J. F. Zhou, T. Koschny, and C. M. Soukoulis, "Magnetic metamaterials at telecommunication and visible frequencies," *Phys. Rev. Lett.* **95**(20), 203901 (2005).
13. J. B. Pendry, A. J. Holden, D. J. Robbins, and W. J. Stewart, "Magnetism from conductors and enhanced nonlinear phenomena," *IEEE Trans. Microw. Theory Tech.* **47**(11), 2075–2084 (1999).
14. K. Aydin, I. Bulu, K. Guven, M. Kafesaki, C. M. Soukoulis, and E. Ozbay, "Investigation of magnetic resonances for different split-ring resonator parameters and designs," *N. J. Phys.* **7**, 168 (2005).
15. R. S. Penciu, K. Aydin, M. Kafesaki, T. Koschny, E. Ozbay, E. N. Economou, and C. M. Soukoulis, "Multi-gap individual and coupled split-ring resonator structures," *Opt. Express* **16**(22), 18131–18144 (2008).
16. V. A. Fedotov, M. Rose, S. L. Prosvirnin, N. Papasimakis, and N. I. Zheludev, "Sharp trapped-mode resonances in planar metamaterials with a broken structural symmetry," *Phys. Rev. Lett.* **99**(14), 147401 (2007).

17. N. Liu, H. C. Guo, L. W. Fu, H. Schweizer, S. Kaiser, and H. Giessen, "Electromagnetic resonances in single and double split-ring resonator metamaterials in the near infrared spectral region," *Phys. Status Solidi B* **244**(4), 1251–1255 (2007).
 18. N. Liu, S. Kaiser, and H. Giessen, "Magnetoinductive and Electroinductive Coupling in Plasmonic Metamaterial Molecules," *Adv. Mater.* **20**(23), 4521–4525 (2008).
 19. M. J. Dicken, K. Aydin, I. M. Pryce, L. A. Sweatlock, E. M. Boyd, S. Walavalkar, J. Ma, and H. A. Atwater, "Frequency tunable near-infrared metamaterials based on VO₂ phase transition," *Opt. Express* **17**(20), 18330–18339 (2009).
 20. E. Cubukcu, S. Zhang, Y. S. Park, G. Bartal, and X. Zhang, "Split ring resonator sensors for infrared detection of single molecular monolayers," *Appl. Phys. Lett.* **95**(4), 043113 (2009).
 21. R. Singh, C. Rockstuhl, F. Lederer, and W. L. Zhang, "Coupling between a dark and a bright eigenmode in a terahertz metamaterial," *Phys. Rev. B* **79**(8), 085111 (2009).
 22. B. Lahiri, A. Z. Khokhar, R. M. De La Rue, S. G. McMeekin, and N. P. Johnson, "Asymmetric split ring resonators for optical sensing of organic materials," *Opt. Express* **17**(2), 1107–1115 (2009).
 23. E. Plum, V. A. Fedotov, P. Kuo, D. P. Tsai, and N. I. Zheludev, "Towards the lasing spaser: controlling metamaterial optical response with semiconductor quantum dots," *Opt. Express* **17**(10), 8548–8551 (2009).
-

1. Introduction

Metallic nanostructures are widely used to generate plasmonic and metamaterial resonances at optical frequencies. Considerable effort has been devoted to designing functional plasmonic nanostructures for applications in biology, energy and communications. For such applications, it is of great importance to be able to control resonant frequencies via nanoscale design of plasmonic resonators. Further, arrays of coupled plasmonic nanostructures and metamaterials can give rise to more complex resonant phenomena such as plasmon resonance hybridization [1–5], Fano resonances [6,7], and plasmonic mimicks for electromagnetically induced transparency [8–11]. Breaking the symmetry of metallic nanostructures such as nanoparticles and nanocavities allows access to different resonant modes that are not readily accessible symmetric configurations. In so doing, arrays of coupled nanoscale resonators can outperform those of conventional single nanostructures by, e.g., enabling narrower resonance line widths. Metamaterials exhibit artificial electric and magnetic responses, and are comprised of resonant elements much smaller than the incident electromagnetic wavelength. At optical frequencies, due to the inherent nanoscale size of metamaterials and the challenges of nanofabrication, resonator elements are of necessity topologically much simpler than their low-frequency counterparts. A commonly used metamaterial element at near-infrared wavelengths is a U-shaped resonator [12], which is a simplified version of a more complex double split-ring resonator (SRR) initially introduced by Pendry for operation at microwave frequencies [13]. Split-ring resonators are commonly used in designing metamaterials over a broad range of frequencies from microwave [13–16] to near infrared [5,12,17–20] wavelengths. At microwave frequencies, the desired electromagnetic response can be achieved with a double SRR design consisting of two concentric strongly coupled asymmetric SRRs. However the available metamaterial electromagnetic designs at near-infrared wavelengths are limited by nanoscale fabrication of resonant elements, i.e., making fabrication of complex shapes very challenging [12]. Split-ring resonators with broken symmetry were shown to exhibit narrow line width resonances yielding high quality factors at microwave frequencies [16] and also subsequently at terahertz [21] and near-IR wavelengths [19,22,23]. A wider range of designs can be accessed in coupled resonators by varying the degree of resonator asymmetry and mutual resonator-resonator coupling strength, which modify the resonant frequencies and field intensities of coupled asymmetric SRRs. In this paper, we articulate alternative metamaterial designs that are achievable using coupled asymmetric SRRs at near-IR wavelengths.

2. Symmetry breaking in planar optical metamaterials

In this study, we used planar SRR arrays as a metamaterial design platform to study the effects of symmetry breaking, coupling strength and resonance hybridization. Figure 1(a) represents the schematic drawing of the unit cell of such a coupled SRR system, consisting of

two SRRs facing each other through their tips, with arm lengths of L_1 and L_2 . Figures 1(b)-1(f) shows scanning electron microscope images of some of the coupled and individual SRR arrays that were investigated both experimentally and numerically. The width of the SRR, $t = 360$ nm; metal width, $w = 150$ nm; in-plane periodicities $a_x = 750$ nm and $a_y = 975$ nm and the metal thickness, $z = 120$ nm are kept constant for all the coupled and uncoupled SRR systems. $100 \times 100 \mu\text{m}$ area arrays of Au SRRs were fabricated on 30 nm ITO coated glass substrates using standard e-beam lithography followed by e-beam Au evaporation and lift-off procedures. 2 nm of Ti layer is deposited as an adhesion layer for Au.

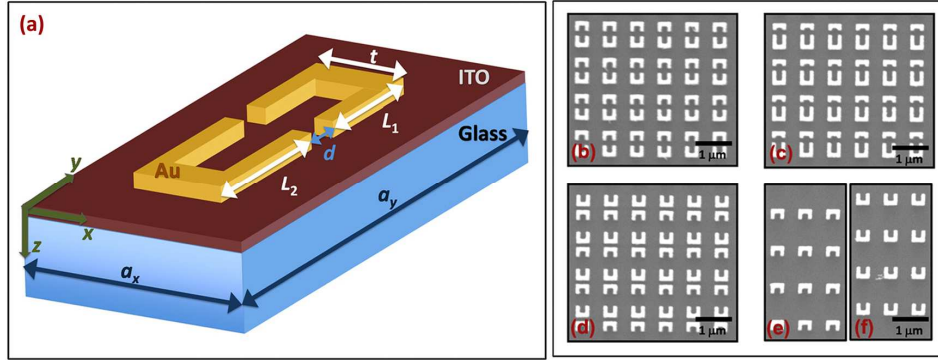


Fig. 1. (a) Schematic representation of a coupled asymmetric split-ring resonator unit cell. (b)-(f) Scanning electron microscope images of coupled and single SRR arrays fabricated by electron-beam lithography.

Transmission spectra of SRR arrays were measured using the Fourier transform infrared microscopy in the wavelength range from 1.4 to $3.2 \mu\text{m}$ using the setup as described in ref [19]. Transmission spectra are normalized to the transmission through a glass substrate of same thickness, assuring that the electromagnetic wave transmission is due only to the response of the metallic metamaterial arrays and thin ITO layer. The electromagnetic wave is normally incident to the SRR plane (k/z) with E -field polarized perpendicular to the SRR arms ($E//x$, $H//y$). (see Fig. 1(a)). Split ring resonators can be modeled as LC resonators in which the effective inductance arises from the loop formed by the U-shaped SRR and effective capacitance is due to the gap region between SRR arms. The LC resonances of SRRs can be excited with an E -field perpendicular to the SRR arms. The resonant response of metamaterial arrays was modeled by full field electromagnetic simulation using a finite-difference time-domain (FDTD) algorithm. Periodic boundary conditions were employed in the simulations along the x and y axes of the single unit cell to mimic a periodic arrangement of SRRs. Along the axis of propagation of the electromagnetic waves, perpendicular to the planar metamaterial layer, perfectly matched layers are utilized. A broadband plane wave is incident on the unit cell along the perpendicular direction, and transmitted power is monitored using a power monitor placed behind the SRR unit cell.

First, we discuss the effect of symmetry breaking on coupled SRR arrays by comparing the measured and calculated frequency response for various symmetric and asymmetric SRR structures. Asymmetry is introduced to the coupled SRR system by changing the length of top and bottom SRRs (L_1 and L_2). The total length of SRR arms, $L = L_1 + L_2 = 580$ nm and the coupling distance between SRRs, $d = 150$ nm are kept same. Scanning electron microscope (SEM) images of the unit cells of 5 different coupled SRR (CSRR) arrays are shown in Fig. 2(c) where the arm lengths of top and bottom SRRs are $L_1 = 290, 310, 340, 370, 400$ nm and $L_2 = 290, 270, 240, 210, 180$ nm, and $d = 150$ nm (from left to right).

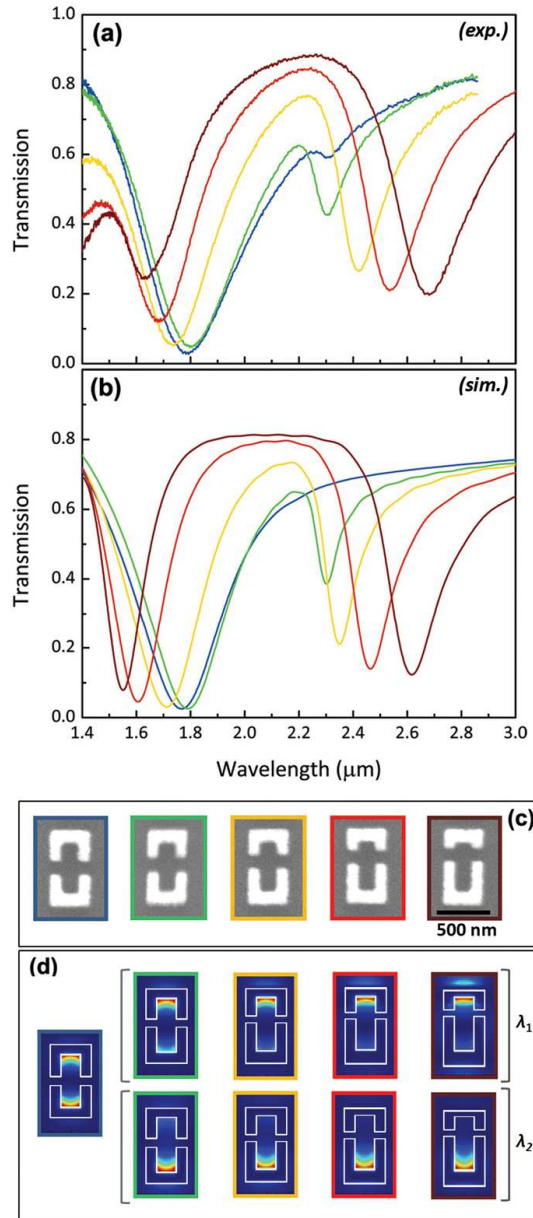


Fig. 2. (a) Measured and (b) simulated transmission spectra of five different coupled SRR systems with $L_1 = L_2 = 290$ nm (blue); $L_1 = 270$ nm, $L_2 = 310$ nm (green); $L_1 = 240$ nm, $L_2 = 340$ nm (yellow); $L_1 = 210$ nm, $L_2 = 370$ nm (red); $L_1 = 180$ nm, $L_2 = 400$ nm (brown). (c) SEM images of single unit cells of corresponding coupled SRR structures (d) Calculated magnetic field intensities of CSRR unit cells at their resonance wavelengths.

Measured and simulated transmission spectra for the corresponding CSRR arrays are plotted in Figs. 2(a) and 2(b) respectively. For the symmetric configuration, a broad resonant dip in transmission spectrum is observed both in the experiments and the simulations (blue line) at $\lambda = 1.78$ μm , which is a typical spectral behavior for a single U-shaped SRR at near-IR wavelengths [12]. In the simulations, we employed the measured values of the complex refractive indices of Ag and ITO layer, which resulted in a very good agreement between the

experimental and numerical results. Changing resonator arm length introduces resonator asymmetry in CSRR arrays, resulting in an additional resonance dip appearing at longer wavelengths. For the asymmetric CSRR with arm lengths of $L_1 = 310$ nm and $L_2 = 270$ nm, the resonance arising due to asymmetry results in a transmission dip in the measured spectra at $\lambda = 2.28$ μm and in the simulated spectra at $\lambda = 2.30$ μm (green line). Interestingly, we observed a very shallow dip in the measured transmission spectra of symmetric SRR arrays (blue line in Fig. 2(a)), which is attributed to unintentional asymmetry that might be introduced during the fabrication process.

Breaking the inherent symmetry in plasmonic nanostructures and metamaterials allows access to different resonant modes, which cannot be excited with the symmetric configuration [2,3,6,16]. Such resonant modes have been termed variously as dark modes, subradiant modes or trapped modes [16]. This nomenclature suggests that dark modes do not readily radiate since they are trapped within the resonator. These modes couple weakly to the free space and needs an external perturbation such as symmetry-breaking of the resonator geometry in order to be excited. In the case of coupled asymmetric SRRs, the narrow line-width resonance with lower losses is due to the anti-symmetric surface currents on each SRR excited by the incident electromagnetic wave [16]. Anti-symmetric currents create fields that interfere destructively resulting in radiation suppression and low-loss light propagation.

The degree of asymmetry is increased further by increasing the difference between arm lengths of the two SRRs in each pair. This results in separation of two resonant frequencies, i.e. blue-shifting of LC resonances at shorter wavelengths and red-shifting of dark-mode resonances at longer wavelengths (yellow, red and brown lines). The separation of the resonance frequencies can be understood with an LC resonance picture. SRRs at near-IR wavelengths are essentially nanoscale LC resonators, and effective inductance arising from the loop formed by the U-shaped SRR and effective capacitance is built up within the gap region between the SRR arms. Changing the physical size of the nanoscale LC resonators results in a change in the effective inductance L and capacitance C . The size change alters the resonance wavelengths of each individual SRR in the coupled SRR system. The resonance wavelengths of the individual SRRs with $L_1 = 310$ nm and $L_2 = 270$ nm (green frame in Fig. 2(c)) are closer than the SRRs with $L_1 = 400$ nm and $L_2 = 180$ nm (brown frame).

We calculated magnetic field intensities along the z -axis ($|H_z|^2$) at the SRR-substrate interface at the resonance wavelengths corresponding to the dip of the transmission resonances (Fig. 2(d)). Under such conditions, magnetic field intensities are enhanced at the center of SRRs, due to the circular surface currents excited by the incident electric field. For the symmetric CSRR, the contributions of the top and bottom SRRs to the dipole moments are equal, hence the same is true for the magnetic field intensities. However, for the asymmetric CSRR systems, the contribution of the longer-armed SRR structure is dominant for the larger wavelength resonance (λ_2) and the shorter SRR dominates the resonance at the shorter wavelength (λ_1) in agreement with the LC resonance description.

The degree of asymmetry is an important parameter controlling the electromagnetic resonant frequency and transmitted intensity. Referring to Figs. 2(a) and 2(b), one can see that the degree of asymmetry also affects the line-width and thus the quality-factor (Q -factor) of both LC and dark-mode resonances. The Q -factor is the ratio of the resonance band-width ($\Delta\omega$) to the resonance frequency (ω), $Q = \Delta\omega/\omega = \lambda/\Delta\lambda$. Here, we define the resonance line width ($\Delta\lambda$) as the full width at half maximum centered at the resonance wavelength (λ). For the symmetric CSRR configuration, the quality factor is calculated from the measured transmission spectra to be $Q \sim 4.0$ at $\lambda = 1.78$ μm with $\Delta\lambda = 0.45$ μm . For the case of CSRR arrays with the lowest degree of asymmetry, quality factors for LC resonances and dark-mode resonances are found as $Q_1 \sim 4.5$ and $Q_2 \sim 23$, respectively. Metamaterial arrays composed of more highly coupled SRRs possess higher quality factors as compared to a symmetric CSRR configuration. For lower degrees of asymmetry, dark-mode resonances exhibit much higher quality factors than is typically achievable with resonators comprised of lossy metallic

nanostructures at optical frequencies. However, Q for dark-mode resonances decreases with increased degree of asymmetry [16]. Quality factors at dark-mode resonance wavelengths are calculated to be 13, 10 and 7.5 for yellow, red and brown lines, respectively. Here, the quality factors of the resonances are affected by several factors, including material losses due to absorption in metal and ITO layer, losses due to coupling of incident electromagnetic wave with the resonators and deviation from the ideal simulated parameters due to inhomogeneities introduced during fabrication (valid for measured transmission spectra). The resonator quality factors could be further increased by using lower loss substrates, or potentially by adding gain media into the metamaterial arrays. The ability to control the quality factor of resonant elements is important for many applications, especially for biological and chemical sensors, narrow-band transmission/reflection filters and modulators.

3. Structural resonance wavelength tuning by controlling the coupling strength

We have shown that one can change the physical size of SRRs in order to tune the resonance wavelengths of metamaterial arrays. However, it is not easy to manipulate the physical size of a resonator controllably in an active manner after fabrication. Inspired by the concept of coupled harmonic oscillators in classical mechanics in which resonant frequencies depend on the coupling strength, we propose an alternative way for tuning the resonance wavelength of metamaterials by controlling the coupling strength between the resonator elements.

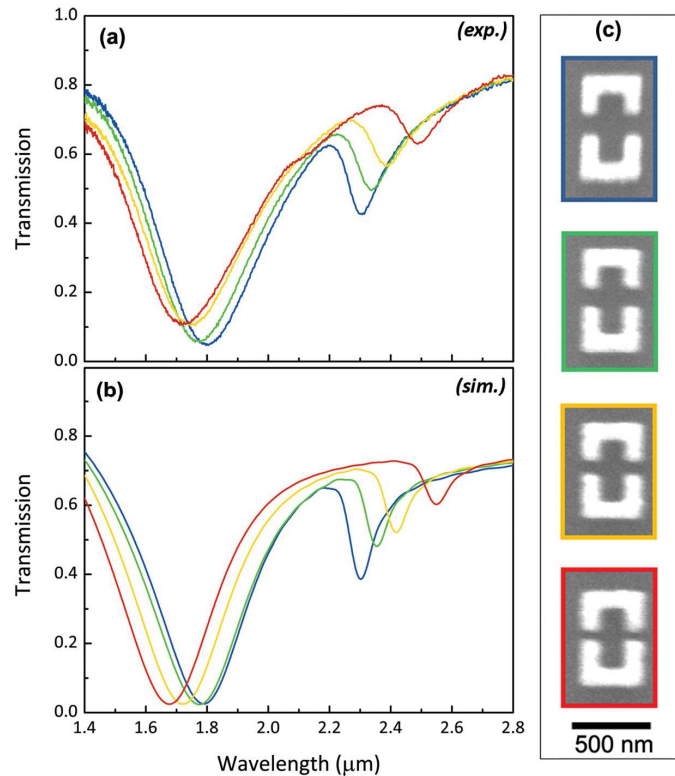


Fig. 3. (a) Measured and (b) simulated transmission spectra of tip-coupled asymmetric SRR arrays with the coupling distance $d = 150$ nm (blue), $d = 120$ nm (green), $d = 90$ nm (yellow) and $d = 60$ nm (red) (c) SEM images of single unit cells of corresponding coupled SRR structures.

In order to understand the effect of coupling in our asymmetrically coupled SRRs, we simply changed the coupling strength by varying the distance between two SRRs. Particularly, we focused on the coupled asymmetric SRR system with the lowest degree of asymmetry for

which $L_1 = 310$ nm and $L_2 = 270$ nm (green in Fig. 2). Four different coupled SRR arrays were fabricated with the distance between SRRs decreasing from $d = 150$ nm to 60 nm with 30 nm steps as seen in Fig. 3(c). Figure 3(a) shows the measured transmission spectra of four different CSRR arrays. The experimental results are in good agreement with the calculations shown in Fig. 3(b). Reducing the coupling distance produces a red-shift of the dark-mode resonance wavelength, and a blue-shift for in LC resonance wavelength. These results agree with the resonance hybridization model in which the resonance energies are shifted from the initial resonance energies of the resonators with increased coupling. The quality factors found from calculated dark-mode resonance spectra are $Q \sim 35$ for trapped mode resonances and ~ 4 for LC resonances for different distances. Therefore the coupling strength does not change the quality factors of CSRRs for 60, 90, 120 and 150 nm coupling distances. However, it is notable that the transmission dip deepens with decreased coupling distance for dark-mode resonances at larger wavelength. This is attributed to the increased phase difference in induced dipole oscillations with the increased coupling strength [5].

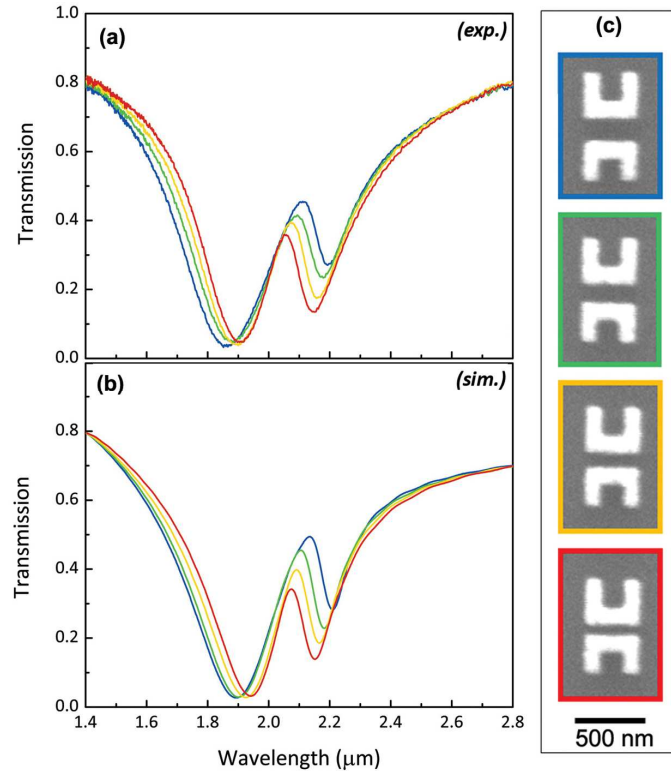


Fig. 4. (a) Measured and (b) simulated transmission spectra of back-coupled asymmetric SRR arrays with the coupling distance $d = 150$ nm (blue), $d = 120$ nm (green), $d = 90$ nm (yellow) and $d = 60$ nm (red) (c) SEM images of single unit cells of corresponding coupled SRR structures

We also studied the effect of coupling for a different geometrical array layout scheme, in which asymmetric SRRs are placed back-to-back, as shown in Fig. 1(d). The dimensions of two coupled asymmetric SRRs are kept same as for the tip-coupled SRR structures in Fig. 3 and the coupling distance between two SRRs are varied from $d = 150$ nm to 60 nm (Fig. 4(c)). The measured and simulated transmission spectra for back-to-back coupled SRR arrays is given in Figs. 4(a) and 4(b). For $d = 150$ nm, the resonance wavelengths are much closer compared to tip-coupled SRR system (blue lines). Reducing the coupling distance between SRRs causes blue-shifts for dark-mode resonances and red-shifts for LC resonances. This

observed behavior is different than the previously observed tip-coupled SRRs for which the change in coupling distance resulted in an increase of dark-mode resonance. Here, we observe an electromagnetically-induced transparency (EIT)-like resonance, since the resonance wavelengths of bright and dark modes come closer with reduced coupling distance in side-coupled SRR. A transmission band is observed similar to those previously reported for electromagnetic plasmonic and metamaterial analogues of EIT-like resonances [8,11].

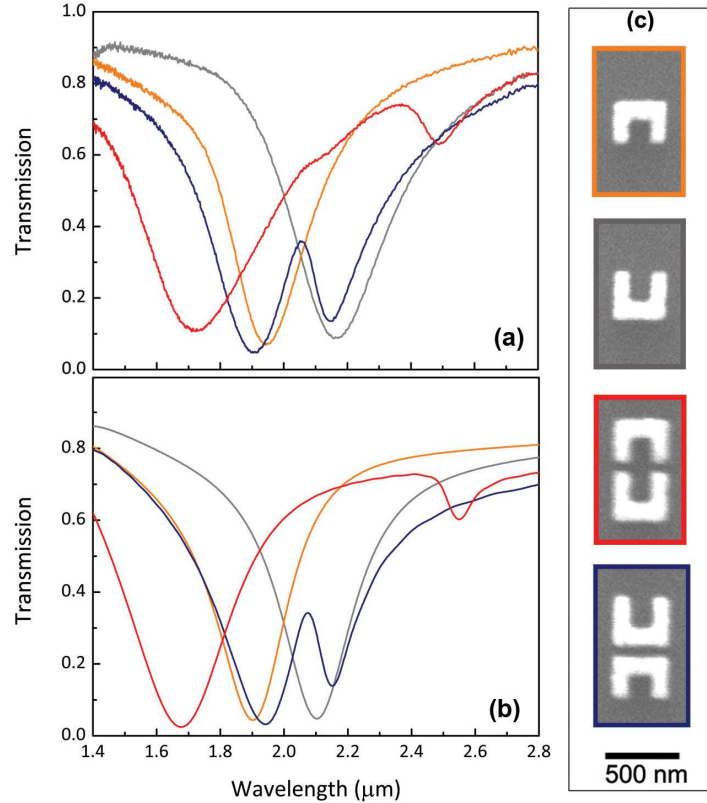


Fig. 5. (a) Measured and (b) simulated transmission spectra of short SRR, long SRR, tip-coupled and back-coupled SRR plotted for comparison with their unit cell shown in (c).

The physics of coupled SRRs can be described in the resonance hybridization picture. Two resonators that initially have different resonance frequencies can be coupled in hybridized resonant modes [1,5]. To better understand asymmetrically coupled SRRs in a resonance hybridization framework, we performed additional measurements and simulations for individual SRRs. Single SRR arrays with $L = 310$ nm and 270 nm are fabricated and simulated. The shorter SRR (orange lines in Fig. 5) is resonant at 1.92 μm , whereas the larger SRR (gray lines on Fig. 5) is resonant at 2.16 μm . In Figs. 5(a) and 5(b), we plot uncoupled SRR resonant wavelengths together with those for tip-coupled and back-coupled SRRs. It is evident that for the back-to-back coupled SRRs, the resonance wavelengths of the coupled system are almost the same as the resonance wavelengths of individual uncoupled SRRs. This indicates that the coupling between back-to-back SRRs is very weak, although they are only separated by 60 nm. However the resonance wavelengths for tip-coupled SRRs 60 nm apart are strongly modified from the original resonance wavelengths due to the strong coupling at small distances.

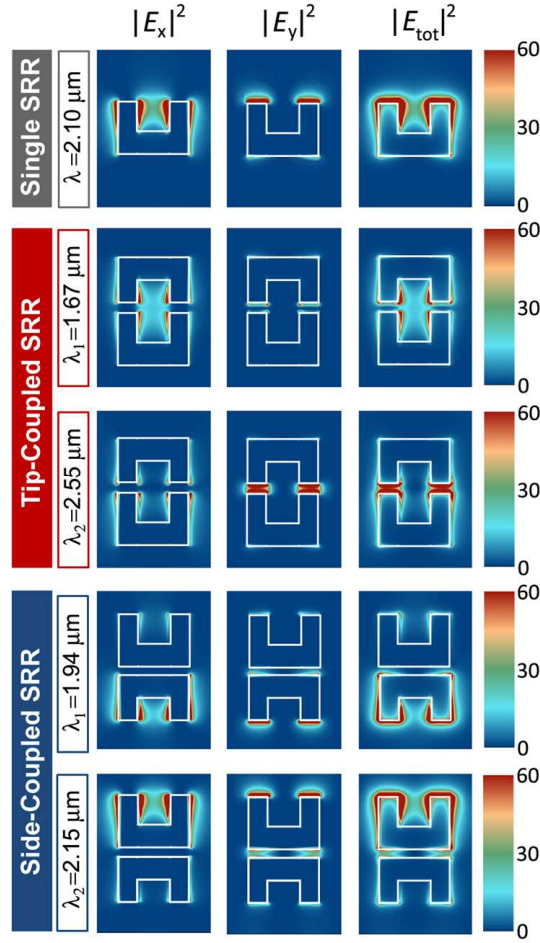


Fig. 6. Calculated electric field intensities $|E_x|^2$, $|E_y|^2$, $|E_{\text{tot}}|^2$ for uncoupled (first row), tip-coupled (second and third row) and back-coupled (fourth and fifth row) SRR.

We calculated the electric field intensities $|E_x|^2$, $|E_y|^2$ and $|E_{\text{tot}}|^2$ for individual, tip-coupled and side-coupled SRR at their resonance wavelengths as shown in Fig. 6. For the single SRR structure (top row), electric fields are localized around the tip region. $|E_x|^2$ is enhanced in the SRR gap region, whereas $|E_y|^2$ is much stronger at the tip of SRR. Strong coupling is evident for the tip-coupled SRRs (second and third rows) and the field intensities in asymmetric CSRRs are comparable. However for the side-coupled SRRs (fourth and fifth rows), fields are much stronger in one of the coupled SRRs. The unit cell of periodic arrays of back-coupled SRRs can alternatively be defined as a set of tip-coupled SRRs with a very large separation distance between coupled resonators as shown in Fig. 7(a). For a complete picture of electric field intensities, we performed several calculations where the distance between tip-coupled SRRs varied between 30nm and 360 nm in 30 nm steps. Maximum electric field intensities along x and y directions for two resonance wavelengths are plotted in Fig. 7(b).

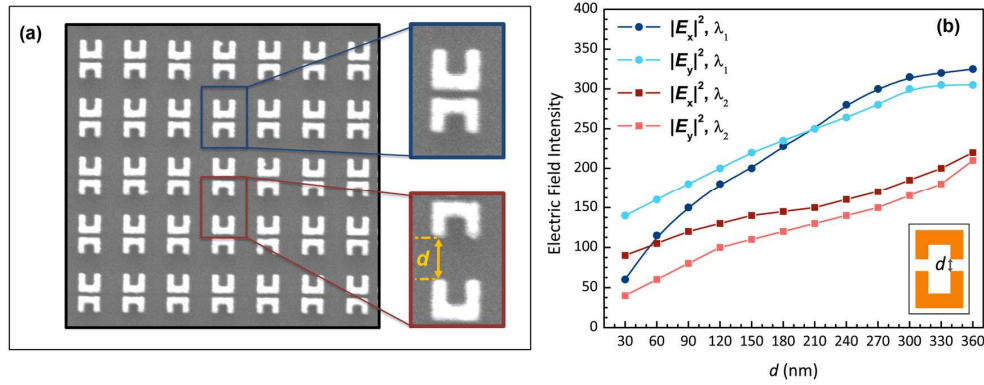


Fig. 7. (a) Back-to-back coupled SRRs can also be considered as long-range tip-coupled SRRs, (b) The maximum value of $|E_x|^2$ and $|E_y|^2$ at resonance wavelengths λ_1 and λ_2 as a function of the d between two tip-coupled SRRs.

In Fig. 8, we plotted the measured and simulated resonance wavelengths of coupled SRRs as a function of the distance between resonators. The gray and orange dashed lines correspond to the resonance wavelengths of long and short SRRs, respectively. For large distances, the coupling effect is very weak; indeed the resonances appear at the original uncoupled resonance wavelengths. However, for smaller distances we observe strong resonance hybridization between the asymmetric SRRs. Experimental (red triangle) and simulated (blue circle) results agree very well. The smallest coupling distance we fabricated was 60 nm. Since, the resonance wavelength increases drastically at very small distances, we performed simulations in order to predict the resonance wavelength of CSRRs with coupling distances of 10 and 30 nm. For a 10 nm distance, the resonance wavelength shifted up to 3.62 μm . A schematic of resonance hybridization is given in Fig. 8(b). Time snapshots of the electric field amplitudes along x direction at resonance wavelengths of individual and coupled SRRs (for $d = 60$ nm) are also provided. Individual SRRs have resonance frequencies ω_1 and ω_2 . Due to resonance hybridization, we observe both symmetric and anti-symmetric modes for the coupled SRR system.

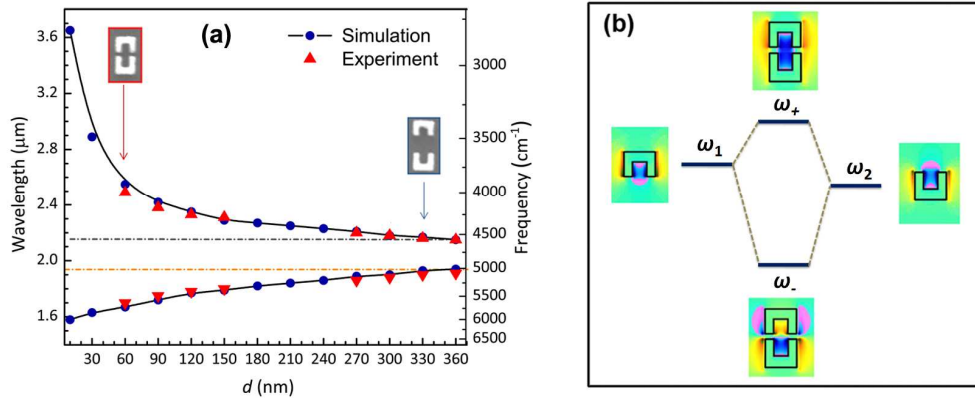


Fig. 8. (a) Measured and calculated resonance wavelengths of different tip-coupled SRRs as a function of distance. (b) Resonance hybridization picture for a strongly coupled asymmetric SRRs. Time snapshot of electric field amplitudes are also provided for the corresponding resonance energies.

Asymmetric coupled SRR design is advantageous in achieving narrower spectral line widths at the resonance frequency, which may find application in frequency selective surfaces for modulators, filters and sensors at infrared wavelengths. For practical applications, it is

desirable to tune the resonance over a wavelength range comparable to its line width, and so a narrower resonance can increase the tuning figure of merit (FOM), the ratio of the tuning range to the FWHM of the resonant peak.

Acknowledgements

This work was supported by the DOE Office of Basic Energy Sciences 'Light-Material Interactions in Energy Conversion' Energy Frontier Research Center under grant DE-SC0001293 (HAA and KA), and in part by the Army Research Office (IMP); portions of this work were performed in facilities sponsored by the Center for Science and Engineering of Materials, an NSF MRSEC. We gratefully acknowledge critical support and infrastructure provided for this work by the Kavli Nanoscience Institute at Caltech. IMP acknowledges the support of a National Science Foundation Graduate Fellowship. We also gratefully acknowledge the help of Professor George Rossman for IR facilities and measurements.